Journal of the European Ceramic Society 20 (2000) 57–66

Evaluation of the thermal shock behaviour of tape cast ceramic substrates by means of lamp irradiation

V. Knoblauch [a, b,*], G. A. Schneider [b], G. Schneider [c], H. Böder [a]

[a] *Robert Bosch GmbH, Abteilung FV/FLW, Postfach 106050, 70049 Stuttgart, Germany*
[b] *Technical University Hamburg–Harburg, Advanced Ceramics Group, Germany*
[c] *Polytechnic Aalen, Germany*

Received 10 November 1998; received in revised form 6 March 1999; accepted 13 March 1999

Abstract

Thermal shock behaviour of tape-cast Y-PSZ is characterised by lamp irradiation, i.e. the generation of strong lateral temperature gradients in thin circular discs by rapid heating with a high power halogen lamp. The accuracy of the method could be strongly improved by coating the samples with a circular graphite spot in the disc centre. This remarkably reduces the elliptical distortion of the temperature profile due to the plane wound filament of the lamp. The time resolved in situ measurement of the temperature profile with a high speed thermal imaging system enables the calculation of the arising thermal stresses. The application of the maximum temperature in the disc centre at the moment of failure, T_{max}, as an easily measurable thermal shock quality control parameter for industrial applications is demonstrated and the relation between T_{max} and the thermal shock resistance parameter under plane stress conditions is discussed. The results are compared with ring-on-ring strength tests which show the same trend.

Keywords: Strength; Thermal shock resistance; ZrO_2; Substrates

1. Introduction

Precise thermal shock evaluation of ceramic materials is still a problem for many reasons.[1] One being that a commonly accepted method is not available which may be due to the fact that the failure criterion depends on the application.

Traditionally, heated samples are quenched in water or other cooling agents and the retained strength of the samples e.g. bending bars is measured.[2] The method is easily performed and allows a precise determination of the applied temperature difference. But the determination of the thermal stresses in quench experiments is difficult and requires a great deal of numerical and experimental investigations to determine the time-dependent temperature distribution.[3–5] Furthermore, size effects of the samples have to be taken into account and make a quantitative evaluation of the data more difficult.[6]

On the other hand, irradiation methods, i.e. a defined transient heating of samples whether by laser beam or halogen lamps are well defined thermal shock tests which allow a precise evaluation of the developed thermal stresses due to in situ measurement of the temperature distribution on the samples surface.[7–14] Samples used are thin circular discs which makes this method especially attractive for thermal shock testing of ceramic substrate materials. Up to now, testing ceramic substrates is performed by quench tests and fracture of specimens or the first occurrence of cracks is correlated with the applied temperature difference.[15] Moreover, substrates are dipped into hot liquid media to examine cracking and fracture of the samples depending on the mediums temperature.[16] However, because the resulting temperature distribution is not known quantitative analysis of the thermal stresses is impossible. Besides, often more preparation effects like for example the quality of specimens edges or the substrates design are tested than the materials properties.

Regarding the relatively simple experimental set-up and the precise controllable halogen lamp used as irradiation source, the "lamp irradiation method" seems

* Corresponding author. Tel.: +49-711-811-7924; fax: +49-711-811-7616.
E-mail address: volker.knoblauch@de.bosch.com (V. Knoblauch).

0955-2219/99/$ - see front matter
PII: S0955-2219(99)00069-2

to be a useful testing tool to characterise the thermal shock behaviour of ceramics in material development. If it succeeds to find an easily measurable parameter that describes the thermal shock behaviour of the substrates the method can be used even in quality assessment in production process.

The objective of this work is first to demonstrate some improvements of the method that could be realised by a special preparation of the samples and by use of a high speed thermal imaging system. In a second step, the applicability of the "lamp irradiation method" as a tool to reliably assess the thermal shock resistance of industrially produced partially stabilised zirconia (PSZ) ceramic substrate materials is shown.

2. Experimental

2.1. Test description

For the experiments a lamp irradiation thermal shock cell similar to the thermal shock equipment developed by Schneider[7] is used.

The thermal shock is generated by irradiating the centre of a circular disc one-sided with a 150 W tungsten halogen lamp. The higher thermal expansion in the disc centre is constrained by the cooler edge causing tangential and radial compressive stresses in the hot zone and tensile hoop stresses in the outer rim. When the thermal stresses in the specimen reach materials strength the sample is destroyed by unstable crack propagation. The temperature distribution at the moment of fracture is measured with a thermal imaging system. The knowledge of the temperature distribution at the moment of failure together with the material properties, i.e. Young's-modulus E, Poisson ratio ν and the thermal expansion coefficient α enables to calculate the thermal shock fracture stress.

2.2. Sample preparation

Circular discs of Y_2O_3 doped partially stabilised zirconia (Y-PSZ) with a diameter of about 25 mm and 0.5 mm thick were punched out of the green tape-cast substrate. After sintering the samples are nearly plane-parallel ($\pm$ 0.02 mm) with a diameter of 20.0 mm and a final thickness of 0.42 mm (because of industrial applications of the materials by the Robert Bosch GmbH, Germany, a more detailed specification is not possible for the moment).

In order to obtain sufficient absorption of the radiation, the surface of the samples was coated with graphite spray. Using uncoated samples it is not possible to induce thermal stresses that reach the mechanical strength of the material and cause fracture of the sample because of the high transmission and reflection of the radiation. Fig. (1) shows the temperature development in the disc centre during thermal loading of coated and uncoated samples.

For the thermal shock investigations the irradiated side of the disc is coated with a circular centred graphite spot with a diameter of 5 mm, the other side is completely coated to ensure a defined emission for the IR-thermometry. To apply the spot at the disc centre a special template is used. The effects of the spot-coating will be pointed out later.

2.3. Thermal shock system

A 150W/15V tungsten halogen lamp situated in the focal point of an ellipsoidal gold coated mirror is used to irradiate the circular samples. The samples are adjusted in the focal plane of the gold coated mirror to achieve maximum irradiation intensity. The lamp is connected to a power supply and operated voltage controlled. A personal computer and the developed software allow a precise time- and voltage-drive of the lamp.

The samples are fixed by two spring loaded alumina pins and one fixed pin to avoid external mechanical constraints. The pins are arranged in an angle of 120°. Because of the short time of the thermal loading (about 2 s) heat dissipation at the pins has not to be taken into account.

In order to realise a precise temperature measurement two independent thermometry systems are used: a thermal imaging system and an infrared pyrometer. The temperature is measured in situ at the unheated completely graphite-coated side. The emission of the graphite was determined to 0.85 for the IR-pyrometer and 0.90 for the thermal imaging system. The thermal imaging system measures in the spectral pass band from 8–12 μm

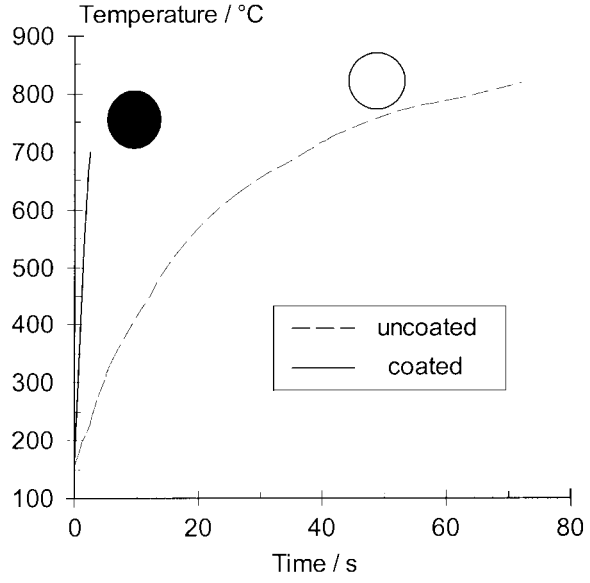

Fig. 1. Different absorption behaviour of graphite-coated and uncoated specimens.

with a relative error < 2%, the IR-pyrometer works in a spectral pass band from 4.5–5.5 μm with a relative error < 10%. These spectral ranges assure that the strongly diffuse scattered light of the halogen lamp (wavelength < 2 μm) from the sample surface does not influence the temperature measurement.

In order to calculate the time dependent thermal stresses at the time of failure the temperature is measured in situ along the horizontal axis of symmetry (linescan-modus) with a frequency of 625 Hz. The procedure is based on the assumption that there is an axisymmetric temperature distribution. Using the whole measuring range of the thermal imaging system (−40 to 1800°C) to register the entire temperature profile the resolution is not sufficient for an exact calculation of the thermal stresses. Therefore the measuring range is limited from 20 to 500°C and the maximum temperature in the disc centre is measured by the IR-pyrometer. The temperature range between 500 and 1000°C is calculated using spline functions.

Fig. (2) shows a schematic diagram of the entire thermal shock equipment.

2.4. Thermal shock testing

Two experiments are carried out with each sample. The first thermal loading — a short flash at a voltage of 15 V and a period of about 0.8 s — is done to assess the temperature profile during the irradiation and to ensure an exact positioning of the disc with regard to the maximum temperature at the disc centre and the symmetry of the temperature field. The temperature is measured two-dimensionally with the thermal imaging system. The accuracy of the positioning depends on the optical resolution of the thermal imaging system according to the combination of lenses and intermediate rings which is about 200 μm in this case.

For the thermal shock test the specimens are irradiated until they are destroyed by unstable crack propagation in order to determine the thermal shock fracture stress. The temperature is measured with the thermal imaging system in the linescan-modus as well as with the IR-pyrometer which determines the maximum temperature at the disc centre, as described in the previous chapter. The thermal imaging system with its good spatial resolution and its high scanning rate (up to 1250 Hz) enables a very precise temperature measurement of the transient heating process.

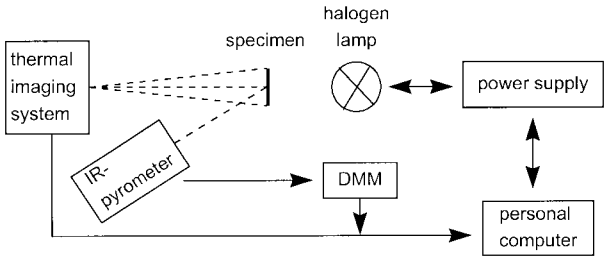

Fig. 2. Schematic diagram of the entire thermal shock equipment.

3. Results and discussion

3.1. Temperature profiles and stress calculation — Influence of the graphite-coating

The temperature profile, respectively the stress distribution, decisively depends on the kind of graphite coating. Hence, we want to attach importance to this effect first.

Because of the plane spiral-wound tungsten filament situated in the focal point of an ellipsoidal gold-coated mirror the temperature field in the focal plane of the lamp is not ideally axisymmetric; it is distorted elliptically. Fig. 3(a) and 3(b) show images recorded by the thermal imaging system during the irradiation of two samples at a voltage of 15 V after 0.8 s. In Fig. 3(a), the completely graphite-coated sample, the elliptical distortion is obvious. In Fig. 3(b) only the centre of the disc was graphite-coated with a spot of 5 mm diameter. The corresponding temperature distribution is almost circular.

Comparing the temperature profiles measured during a short flash along the horizontal (x) and vertical (y) axis of symmetry of the discs using the linescan-modus [Fig. 4(a) and 4(b)] we recognise approximately identical temperature profiles in both directions for the spot-coated sample. The temperature gradient is very similar, the maximum difference in temperature between the x- and y-linescan is only about 20 K. However, the completely coated disc has different temperature gradients in x- and y-direction and maximum differences up to 60 K. The temperature measurement along the y-axis is influenced by the alumina pin which is situated in the y-axis. Therefore, the specimens rim could not unambiguously be detected. This causes the seeming temperature increase at the outer rim.

The corresponding in-plane stress fields are pointed out in Fig. 5(a) and 5(b). Only the tangential components are looked at because tensile stresses are considered to be responsible for the failure of ceramics. The radial components are compressive during the thermal loading all over the sample and therefore assumed to be uncritical for the failure. The stress calculations are based on the assumption of an axisymmetric temperature field and a plane state of stress. Because of the small thickness and the little thermal mass of the specimen an axial temperature gradient causing bending stress is neglected.[17] The material properties, i.e. Young's modulus E, Poisson ratio ν and the thermal expansion coefficient α are taken independent on T.

The stress distributions are related to the temperature distribution $T(r)$ by

$$\sigma_t(r) = \alpha.E.\left[1/a^2\int_0^a T(r)r\mathrm{d}r + 1/r^2\int_0^r T(r)r\mathrm{d}r - T(r)\right] \quad (1)$$

for the tangential stress, and

$$\sigma_r(r) = \alpha E\left[1/a^2\int_0^a T(r)r\mathrm{d}r - 1/r^2\int_0^r T(r)r\mathrm{d}r\right] \quad (2)$$

for the radial stress, where a is the radius of the sample and r the radial position.[18] The calculations are carried out by use of the FE-codes I-DEAS (SDRC, Structural Dynamics Research Corporation, Milford, OH, USA) and ABAQUS (Hibbitt, Karlsson & Sorensen, Inc. Pawtucket, USA) using an axisymmetric finite-element model.

Fig. 5(a) and 5(b) show the distribution of the tangential stresses according to the temperature profiles shown in Fig. 4(a) and 4(b). There is a significant difference in the stress distribution over the whole diameter whether the calculation is based on the temperature profile along the x- or along the y-axis regarding the completely coated specimen. The maximum difference amounts to 35 MPa at a radius r of 5–6 mm. For the spot-coated specimen

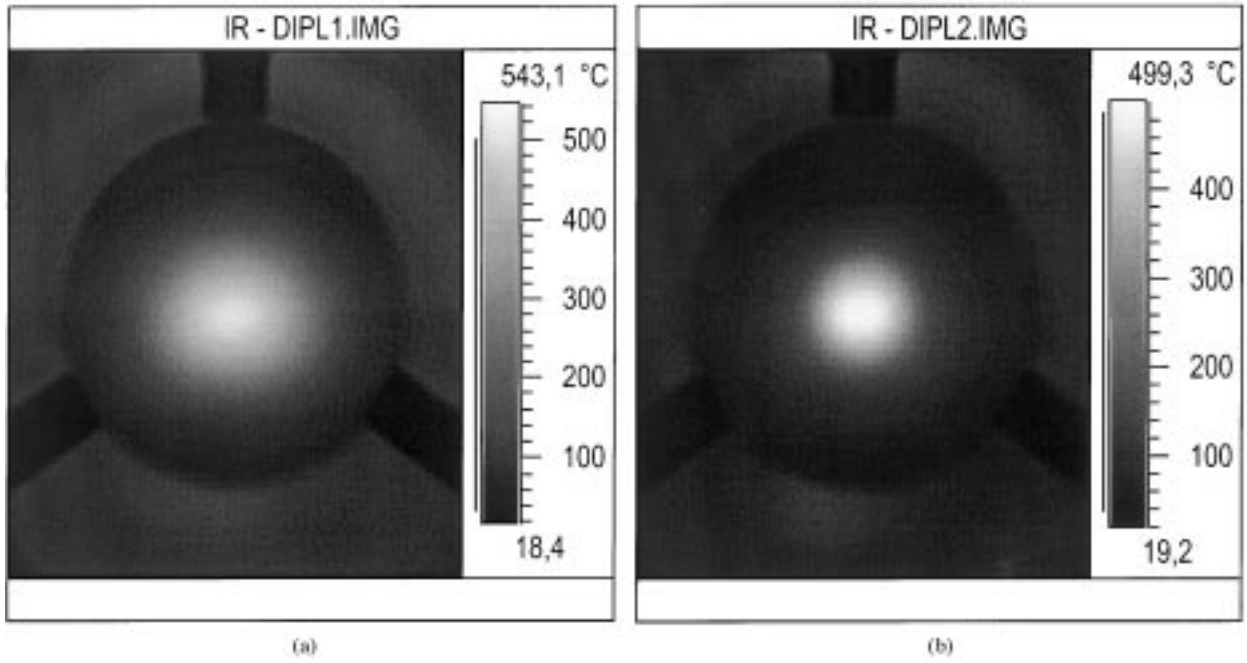

Fig. 3. (a): 2-dimensional temperature distribution of a completely coated sample after 0.8 s of irradiation at a voltage of 15 V; (b): 2-dimensional temperature distribution of a spot-coated sample after 0.8 s of irradiation at a voltage of 15 V.

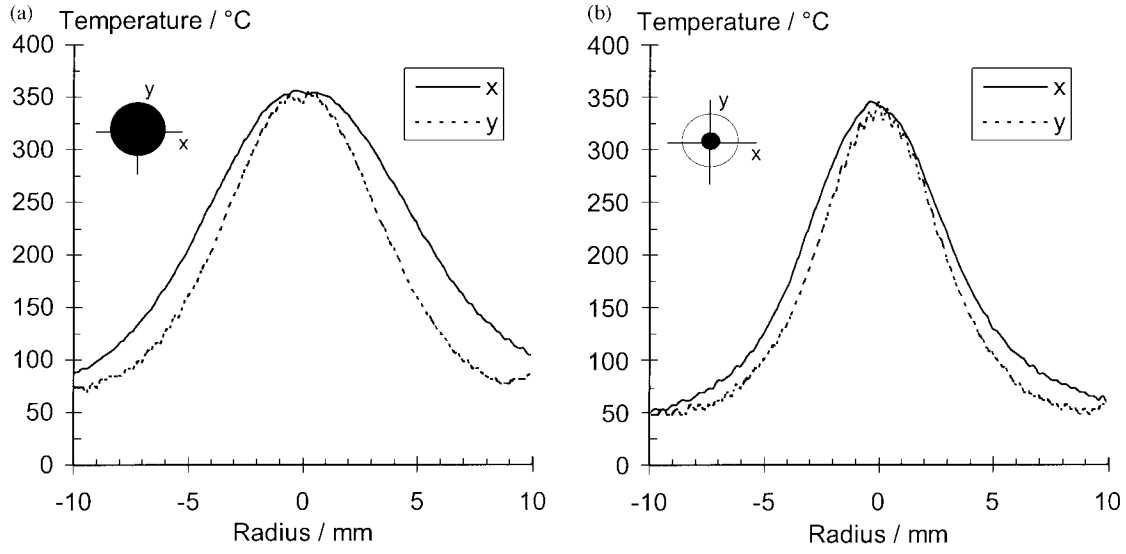

Fig. 4. (a): Temperature profile along the horizontal (x) and vertical (y) axis of symmetry of a completely coated disc after 0.8 s at a voltage of 15 V; (b): Temperature profile along the horizontal (x) and vertical (y) axis of symmetry of a spot-coated disc after 0.8 s at a voltage of 15 V.

the stress profiles are almost identical [see Fig. 5(b)]. The stress distribution at the outer rim is influenced by the seeming temperature increase at the specimens rim for the y-axis. Therefore, the decrease of the stress is not as big as it is shown.

For the following considerations the temperature profiles along the horizontal axis of symmetry form the basis of the calculations.

Regarding the temperature- and stress distributions of a completely and a spot-coated disc at the time of failure considerable differences could be recognised, too.

The maximum temperature at the disc centre is substantially higher ($\Delta T = 250\,\mathrm{K}$) and the temperature gradient is steeper for the spot-coated sample than for the completely coated one. At the outer rim the temperature profiles are similar, as shown in Fig. 6(a). The resulting thermal stresses are plotted in Fig 6(b). In case of spot-coating the compressive stresses in the disc centre are about $-700\,\mathrm{MPa}$ and are approximately 2 times higher than for the completely coated one. The change-over from the compressive- to the tensile-stress region occurs at a radius r of 3 mm. Hence, the tensile stress loaded volume amounts to 90% of the entire volume

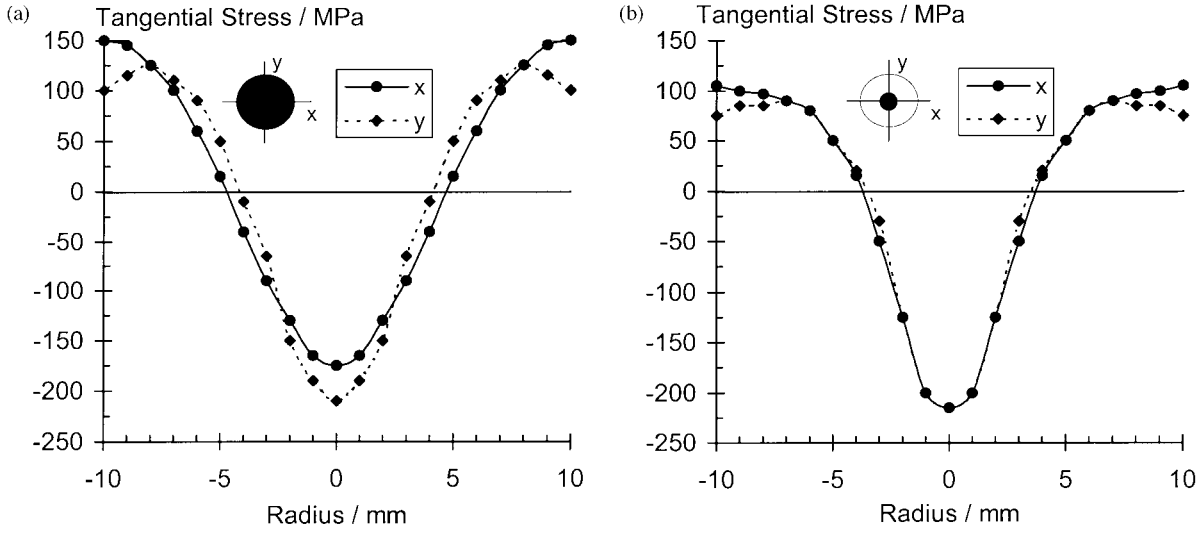

Fig. 5. (a): Distribution of the tangential stresses of a completely coated sample along the horizontal (x) and vertical (y) axis of symmetry after 0.8 s of irradiation at a voltage of 15 V; (b): reduction of the elliptical distortion of the temperature field by spot-coating (spot diameter = 5 mm): distribution of the tangential stresses along the x- and y-axis of the disc after 0.8 s of irradiation at a voltage of 15 V.

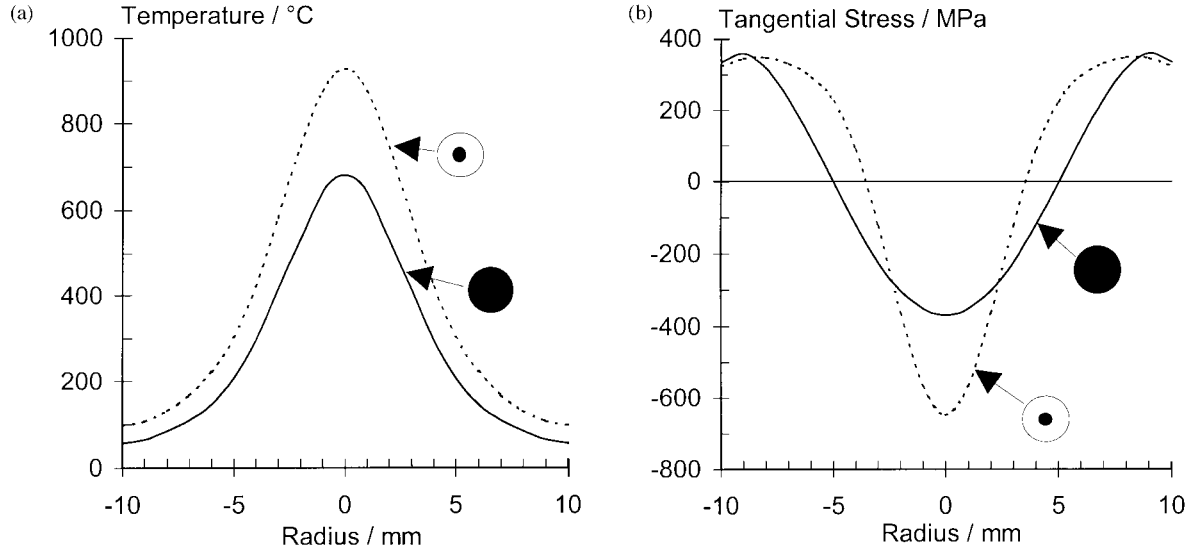

Fig. 6. (a): Temperature profiles of a completely and a spot-coated sample at the time of failure; (b): distribution of the tangential stresses of a completely and a spot-coated sample at the time failure.

of the sample. For the completely coated one it is approximately 70%. In both cases the maximum tangential stress occurs at a radius of 8–9 mm and not at the outer rim. Remarkable is the seeming low fracture strength of the Y-PSZ of about 300–350 MPa.[19–21] We will attach importance to this phenomena later.

Comparing the temperature in the disc centre of different samples after an irradiation of 0.8 s at a voltage of 15 V only a small scatter of about ± 10 K corresponding ± 3% is visible. This demonstrates the very good reproducibility of the test. However a large scatter of the maximum temperature at the time of failure is observed, due to the strength distribution of the samples.

3.2. Evaluation of the thermal shock resistance of Y-PSZ by measuring the maximum temperature at the disc centre, T_{max}, at the moment of failure

The tangential stresses in the disc are given by Eq. (1). Assuming that failure will happen at the position r_0 that is under maximum loading the thermal shock resistance parameter under plane stress conditions $R^* = R(1-\nu)$[2] can be determined instantly by dividing Eq. (1) by α and E and solving the integral without the knowledge of α and E.[14] Thus R^* is given by

$$\sigma_t(r=r_0)/\alpha E = \left[1/a^2\int_0^a T(r)r\mathrm{d}r + 1/r_0^2\int_0^{r_0} T(r)r\mathrm{d}r - T(r)\right] = R^* \quad (3)$$

This procedure requires to measure the whole temperature profile at the moment of failure $T_f(r)$ either by a high speed scanning pyrometer or by a thermal imaging system. Considering just small variations in the composition of the investigated samples and therefore only slight deviations in the thermal conductivity, the specific heat, and the density and assuming the boundary conditions to be constant, the temperature distribution at the time of failure may be expressed as $T_f(r) = T_{\max}\cdot\hat{T}(r)$ where $\hat{T}(r)$ is approximately identical for all specimen with similar composition.

Under this condition Eq. (3) can be transformed to

$$\sigma_t(r=r_0)/\alpha\cdot E = T_{\max}\cdot b = R^* \quad (4)$$

and

$$b = 1/a^2\int_0^a \hat{T}(r)r\mathrm{d}r + 1/r_0^2\int_0^{r_0}\hat{T}(r)r\mathrm{d}r - \hat{T}(r)$$

becomes constant.

Therefore, we conclude that $T_{\max}$ is directly proportional to the figure of merit R for our samples. Because R^* and $T_{\max}$, respectively, is proportional to the fracture strength we evaluate our $T_{\max}$ data by a Weibull distribution according to

$$P_f = 1 - \exp[-(T_{\max}/T_0)^m] \quad (5)$$

where P_f describes the failure probability and T_0 the Weibull parameter corresponding to a failure probability of 63.2%.

Fig. 7(a) shows the Weibull statistics of one batch of Y-PSZ divided in two lots. One part has artificial edge defects made by a grindstone, the other part is tested as sintered. Apparently the two lots can be distinguished clearly, both by the Weibull modulus and the Weibull parameter T_0. But there are only four samples with large macroscopic edge defects [see Fig. 7(b)] that fracture at very low temperatures. Specimens with only small edge

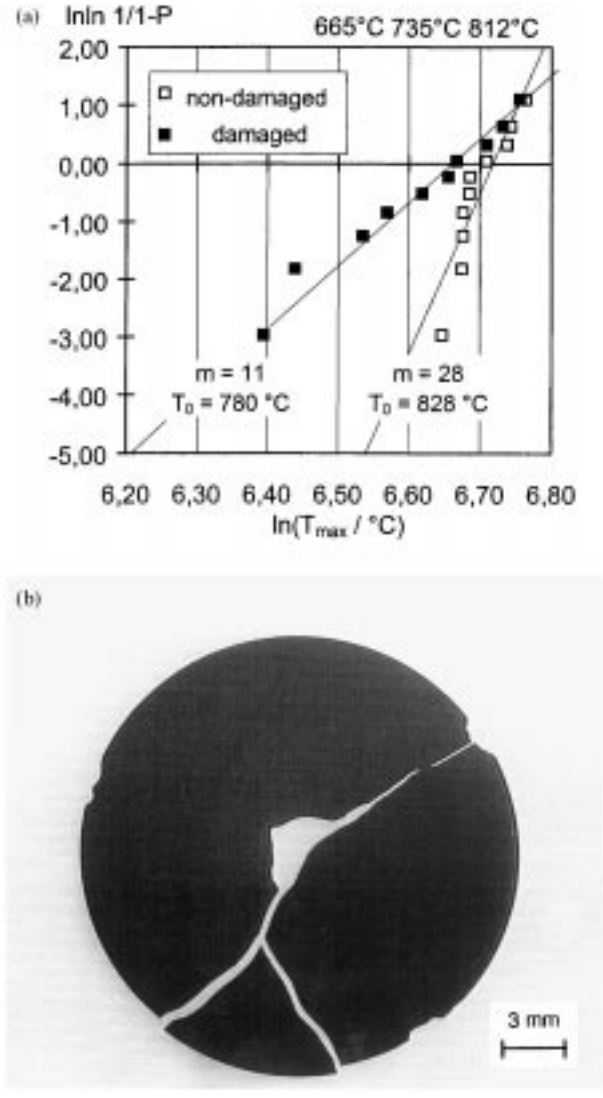

Fig. 7. (a) Weibull-plot of $T_{\max}$ of spot-coated samples with artificial edge defects; (b): photograph of a sample with macroscopic artificial edge defects.

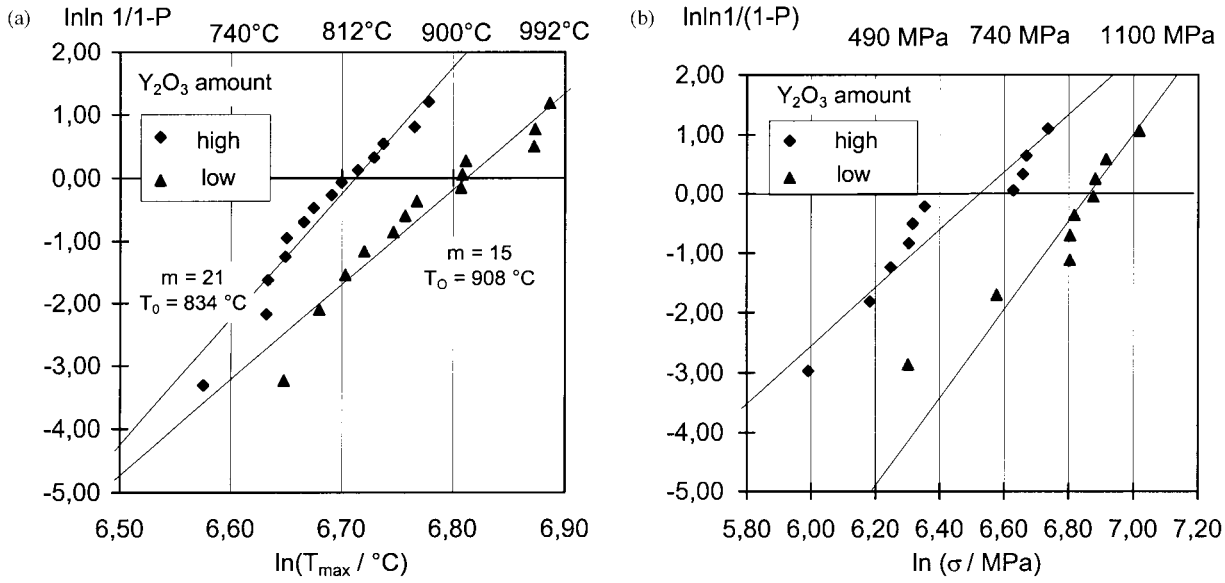

Fig. 8. (a) Weibull plot of T_{max} for two Y-PSZ batches with different amount of Y_2O_3; (b): fracture strength (ring-on-ring test) of the same two Y-PSZ batches as in (a).

defects reach the same level as the undamaged ones. This becomes understandable regarding the stress profile in Fig. 6(b). The maximum tangential stress does not occur at the outer rim but at a radius of 8.5 mm. Hence, we can conclude that the test is not sensitive to small edge defects and only severe damage will influence the results. Thus, the specimens can be tested as sintered.

In Fig. 8(a) the Weibull-plot of two Y-PSZ batches with slightly different amounts of Y_2O_3 is shown. We found a significant difference in the Weibull parameter T_0. There is no significant difference in the Weibull modulus regarding the 90% confidence interval. The correlation is confirmed by results of the fracture strength determined by a ring-on-ring test [see Fig. 8(b)]. We find a decrease of the fracture strength with an increase of the additive level as described in literature.[19,22]

Table 1 shows the ratios of R^*, T_{max} and b calculated by means of the measured temperature distribution of each batch. The indices qualitatively describe the Y_2O_3 amount.

Unfortunately b in Eq. (4) is not constant and changes as much as T_{max}. In general this change of b excludes to use T_{max} as a measure for R^*. In our case b changes in the same direction and scale as T_{max}. Therefore, if we compare T_{max} values we underestimate the change of R^* and reduce the resolution of the test. But obviously the resolution is high enough two distinguish clearly between two Y-PSZ batches with a difference of only 2-wt% of Y_2O_3. Thus, we may use T_{max} as a measure for the thermal shock resistance and as a simple tool for the quality control of our Y-PSZ batches. Because the development of b is not instantly obvious for different materials and compositions it has to be evaluated once out of the normalised measured temperature profile.

Table 1
Ratio of R^*, T_{max} and b

	Ratio
R^*_{low}/R^*_{high}	1.19
$T_{max,low}/T_{max,high}$	1.11
b_{low}/b_{high}	1.08

3.3. Influence of the shock specimens thickness on the calculated thermal fracture strength

Testing samples with varying thickness a correlation between the specimens thickness and the calculated fracture strength is identified. The results are shown in Fig. 9(a) and 9(b). Fig. 9(a) shows the temperature profiles of three samples with a thickness of 0.20, 0.35 and 0.55 mm at the time of failure. The thickness increase leads to higher temperatures at the time of failure. In Fig. 9(b) the corresponding tangential stresses are shown. We find that the thicker the specimen the higher the thermal shock fracture stresses are.

Besides, it is remarkable that the change-over from tensile to compressive stresses occurs for every sample at the same radius $r = 3.5$ mm. Obviously, the temperature profiles for discs with different thickness are similar in a wide range. In addition it becomes clear that the deviation of b is not related to the different T_{max} of the batches (see Section 3.2). We find similar temperature profiles and therefore identical values of b even for large

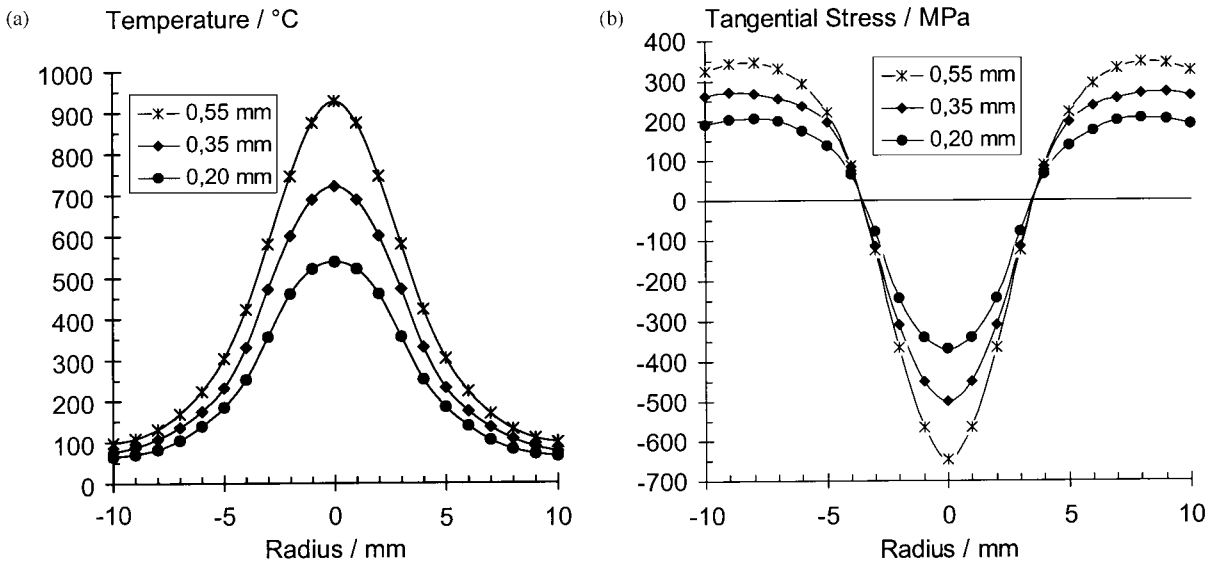

Fig. 9. (a) Temperature profiles of specimens with different thickness at the moment of fracture; (b): corresponding tangential stresses of specimens with different thickness.

differences of T_{max} up to 350 K. Thus, b is only influenced by the materials composition. Hence, a small scatter of the samples thickness will not influence the test regarding T_{max} as a measure of R^*.

The increase of the thermal shock fracture stress for thicker samples is not in consensus with the Weibull theory. Because for thicker samples the stress loaded volume gets higher a decrease of the thermal shock fracture strength would be expected. Fig. 10 shows a comparison of fracture strength obtained by the lamp irradiation method and the ring-on-ring test considering different stress loaded volumes. The effective volume of the ring-on-ring test, calculated analytically using some simplifications for the stress profiles, amounts to about 0.80 mm^3 (radius of inner ring 1.875, radius of outer ring 7.5 mm, Weibull modulus 10, samples thickness 0.40 mm).[23] For $m = 18$ it is about 0.35 mm^3. Assuming plane stress conditions for the discs the effective volume of the thermal shock test is calculated numerically to be about 60 mm^3. The hatched lines in Fig. 10 show the extrapolation of the fracture strength starting from the thermal shock and from the ring-on-ring results regarding the 90% confidence interval of the Weibull modulus. There is no overlay of the fracture strength of the testing methods.

A possible explanation for the seeming low thermal shock fracture stress could be a martensitic tetragonal monoclinic phase transition with volume expansion under thermal loading. Because of that there would be additional stresses which would not have been considered for the thermal stress calculations. But before and after the thermal shock testing 42% cubic and 58% tetragonal modification has been determined by X-ray diffraction (XRD). Hence, there is no phase transition.

Perhaps buckling of the samples due to radial compressive stresses could be a reasonable explanation for the phenomena. Assuming that the failure is not caused by the tangential tensile stresses but rather by the radial compressive stresses that cause buckling of the sample the assumption of a plane state of stress is not permissible. Thus, the deformation of the specimen and the stress distribution at the moment of failure are quite complicated. Detailed FE-calculations have to be carried out for that.

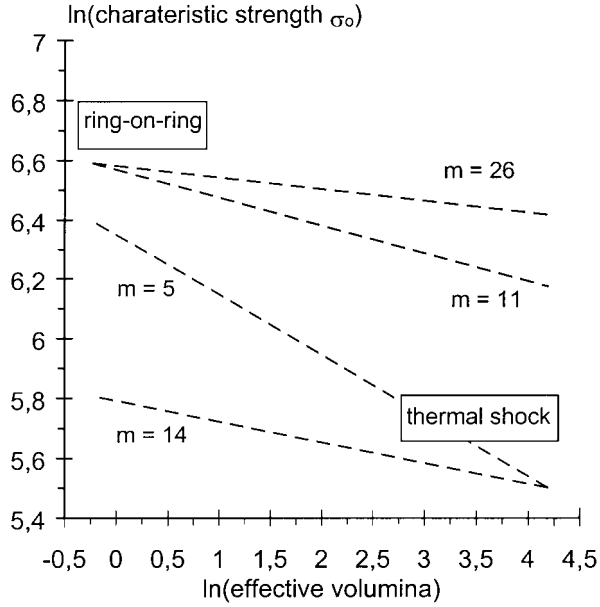

Fig. 10. Comparison of the fracture strength measured by the ring-on-ring test and the lamp irradiation method according to the Weibull theory.

4. Summary

A lamp irradiation thermal shock cell was used to investigate the thermal shock resistance of thin circular discs of tape cast Y-PSZ. Using a thermal imaging system for IR-thermometry enables to measure the two-dimensional temperature distribution in situ during the irradiation of the samples with high precision.

Therefore, it was possible to investigate the elliptical distortion of the temperature field due to the plane spiral-wound filament of the lamp. Its influence on the stress calculation could be pointed out. By coating the specimens with a circular centred graphite spot the elliptical distortion of the temperature field is reduced considerably and an axisymmetric stress calculation becomes very accurate. Furthermore, the tensile stress loaded volume of the sample at the time of failure is increased up to 90% of the entire sample volume. The experimentally measured low thermal shock fracture stresses are due to the big volume tested which leads to an increasing reliability of the test regarding the application of the results on real components.

By varying the diameter of the graphite spot the temperature profiles and therefore the stress distribution of the disc can be adjusted. Therefore, similar possibilities compared to a scanning laser system could be achieved.[13,14] Although testing materials with a high thermal shock resistance like HPSN would be difficult because of the limited power of the halogen lamp, perhaps the use of two lamps could put things right.

Simply measuring the maximum temperature in the disc centre at the moment of failure with an IR-pyrometer we are able to distinguish between Y-PSZ batches with a variation of just 2-wt% in the amount of Y_2O_3. Hence, it is a sensitive method to characterise low variations in composition. If only qualitative differentiation is required this result offers new aspects, e.g. for quality assessment of ceramic substrates in production process and material development. An additional advantage is given by the favourable stress distribution at the moment of failure of a spot coated sample. The maximum tensile stress does not occur at the outer rim. Thus, small edge defects due to the preparation should be uncritical and material properties are determined rather than preparation effects of the samples. Regarding the conventional thermal shock tests of ceramic substrates[15,16] this testing method allows a quantitative analysis of the thermal shock fracture stresses.

Some phenomena which do not correspond with the Weibull theory have been detected. They probably indicate buckling of the samples due to radial compressive stresses. Such effects have not been considered in former examinations in this field.[14,17,24] Further investigations concerning this problem are carried out both in the field of simulation and experiments.[25]

References

1. Schneider, G. A. and Petzow, G. (eds), *Thermal Shock and Thermal Fatigue Behavior of Advanced Ceramics*, NATO ASI Series, Series E, Vol. 241. Kluwer Academic, Dordrecht, The Netherlands, 1993.
2. Hasselman, D. P., Unified theory of thermal shock fracture initiation and crack propagation in brittle materials. *J. Am. Ceram. Soc.*, 1969, **52**, 600.
3. Trantina, G. G., Statistical fracture analysis of brittle materials in thermally stressed components. In *Thermal Stresses in Severe Environments*, ed. D. P. H. Hasselman and R. A. Heller. Blacksburg, VA, 1980, pp. 229–244.
4. Brockenbrough, J. R., Forsythe, L. E. and Rolf, R. L., Reliability of brittle materials in thermal shock. *J. Am. Ceram. Soc.*, 1986, **69**(8), 634–637.
5. Kanto, Y. and Homma, H., Effect of cooling configuration on thermal shock fracture toughness of SiC. *Engineering Fracture Mechanics*, 1991, **40**(4/5), 893–901.
6. Becher, P. F., Lewis III, D., Carman, K. R. and Gonzalez, A. C., Thermal shock resistance of ceramics: size and geometry effects in quench tests. *J. Am. Ceram. Soc. Bull*, 1980, **59**, 542–548.
7. Schneider, G. A. and Petzow, G., Thermal shock testing of ceramics — a new testing method. *J. Am. Ceram. Soc.*, 1991, **74**(1), 98–102.
8. Pompe, W., Bahr, H.-A., Schneider, G. A. and Weiss, H. J., Modelling and measuring of the thermal shock behaviour of ceramics. *Ceramic Forum International*, 1993, **70**(3), 79–84.
9. Schneider, G. A. and Bahr, H.-A., Thermal shock of ceramics. In *The Encyclopedia of Advanced Materials*, ed. D. Bloor, R. J. Brook, M. C. Flemmings and S. Mahajan, Pergamon, 1994, pp. 2822–2829.
10. Magerl, F., Schneider, G. A. and Petzow, G., Crack initiation and crack growth in ceramics under thermal loading. In *Advanced Materials '93, I/A, Ceramics, Powders, Corrosion and Advanced Processing*, ed. Mizutani, Trans. Mat. Res. Soc. Jpn., Vol 14A, Elsevier Science, 1994, pp. 395–399.
11. Schneider, G. A., Magerl F. and Petzow G., Thermal shock and thermal fatigue behaviour of Si_3N_4-ceramics. In *Advanced Materials '93, VI/Frontiers in Materials Science and Engineering*, ed. Somiya et al., Trans. Mat. Res. Soc. Jpn., Vol 19B. Elsevier Science, 1994, pp. 837–846.
12. Magerl, F., Schneider, G. A. and Petzow, G., Crack initiation and crack growth in ceramics and glass under thermal stress. *Ceramic Forum International*, 1996, **73**(4), 235–238.
13. Kirchhoff, G., Thermal shock fracture by laser irradiation. In T*hermal Shock and Thermal Fatigue Behaviour of Advanced Ceramics*, ed. G. A. Schneider and G. Petzow. NATO ASI Series E, Vol. 241. Kluwer Academic, Dordrecht, The Netherlands, 1993, pp. 245–251.
14. Kirchhoff, G., Weiss, H.-J., Holzherr, M., Bahr, H.-A., Pflugbeil, I. and Pompe, W., Characterization of thermal shock and thermal fatigue behaviour of ceramics by means of laser irradiation. In *Proceedings of the First International Symposium on Thermal Stresses and Related Topics*, Shizuoka, June 1995, pp. 119–122.
15. Draft of DIN 41850-1 (German Industry Standard).
16. DE 41 39 166. Patent Specification, Hoechst CeramTec, Germany.
17. Magerl, F., Thermoschock- und thermisches Ermüdungsverhalten von keramischen Werkstoffen unter

bruchmechanischen Aspekten. *Fortschritt-Berichte VDI*. Reihe 18, No. 160. VDI-Verlag, Düsseldorf, 1994.
18. Boley, B. A. and Weiner, J. H., In *Theory of Thermal Stresses*, Robert E. Krieger, FL, 1985.
19. Stevens, R., In *Ceramics and Glasses*. Engineered Materials Handbook, Vol. 4. ASM-International, 1991, pp. 779–784.
20. Wuthnow, H., In *Technische keramische Werkstoffe*, Chapter 9.4.3.1, 1996, pp. 1–8.
21. Hwang, J.-R., Shih, J.-L. and Jeng, M.-C., Fatigue crack growth rate of zirconia ceramics. *J. Mat. Sci.*, 1997, **17**, 1587–1590.
22. McColgan, P., Dransfield, G. P. and Egertont, A., The effect of rare earth oxide additions on the mechanical properties of Ce-TZP. Presented at the 2nd Conference of the European Ceramic Society, 1991.
23. Knoblauch, V., Berührungslose Charakterisierung thermomechanischer Eigenschaften keramischer Werkstoffe. Diploma thesis, Polytechnic Aalen, 1996.
24. Rettig, U., Pompe, W., Bahr, H.-A. and Bast, U., Die Lebensdauer von Si_3N_4-Keramik, ermittelt mit der Laserschock-Methode. In *Fortschrittsberichte der Deutschen Keramischen Gesellschaft*, 1996, **11**(2), 107–114.
25. Knoblauch, V., Schneider, G. A., Dressler, W., Schneider, G. and Jeannel, L., Buckling effects during thermal shock testing of advanced ceramics using irradiation methods. *J. Am. Ceram. Soc.*, in preparation.